Theoretical Model of Rainfall in Tropical Cyclones for the Assessment of Long-Term Risk

By
Andreas Langousis and Daniele Veneziano

Department of Civil and Environmental Engineering, MIT, Cambridge, Mass., USA

Submitted to
Journal of Geophysical Research

Originally Submitted: March, 2008
Revised: October, 2008
Accepted: November, 2008

---

*Corresponding author: Andreas Langousis, Dept. of Civil and Environmental Engineering, MIT, Room 1-245, Cambridge, MA, 02139. Tel: 617-407-0059, andlag@mit.edu.

Abstract

We propose a theoretical model to evaluate the rainfall intensity field due to large-scale horizontal wind convergence in tropical cyclones (TCs). The model is intended as one component of a methodology to assess the risk of extreme rainfall intensities from TCs. The other components are a recurrence relation for the model parameters and track and a statistical representation of the deviations of rainfall intensity from model predictions. The latter are primarily caused by rainbands and local convective activity and is the focus of an upcoming communication. The vertical flux of moisture and the associated surface rain rate are calculated using basic thermodynamics and a simple numerical model for the vertical winds inside the TC boundary layer. The tropical cyclone is characterized by the radial profile of the tangential wind speed at gradient level, the storm translation velocity, the surface drag coefficient, and the average temperature and saturation ratio inside the TC boundary layer. A parametric analysis shows the sensitivity of the symmetric and asymmetric components of the rainfall field to various storm characteristics.

Index Terms: Precipitation (3354), Theoretical Modeling (3367), Tropical Meteorology (3374), Boundary layer processes (3307), Floods (1821).

1. Introduction

Tropical cyclones (TCs) are atmospheric disturbances capable of producing extreme rainfall with devastating social and economic impact (Landsea, 2000; Rappaport, 2000). Consequently, there is much interest in the assessment of the rainfall hazards posed by TCs, either in real time (with leads of hours or days) or in the long run; see e.g. Marks *et al*. (1998). For the latter purpose, when interest is in the rate at which different rainfall intensity levels are exceeded, one needs to parameterize the storms and for each set of parameters evaluate rainfall at the site or over the region of interest as a random process in time or a random field in space-time. In principle, the stochastic rainfall model could be directly fitted to data from historical events, but the large number of parameters and the relative lack of historical data make an empirical model identification and fitting approach unfeasible. Moreover, it would be difficult in such an approach to incorporate knowledge of the physics of the phenomenon. A better approach, which we follow here, is to formulate a physically-based rainfall model. The model should be simple enough that it can be run under a very large set of scenario conditions; hence detailed numerical TC models would not be suited for this purpose.

Neither simple nor sophisticated TC models can produce accurate statistical estimates of space-time rainfall for a given set of global TC parameters. Therefore, any deterministic rainfall model must be complemented by a statistical representation of the rainfall "residuals", defined as the difference between observed rainfall and model prediction. For example, the model developed here ignores the rainfall fluctuations due to rainbands and local convection. The statistical characterization of these fluctuations (residuals) is the focus of a separate communication.

The third and final component of a long-term TC rainfall risk analysis method is the recurrence model, which specifies the frequency with which different TC parameter combinations occur in the region of interest. This component has been the subject of numerous studies, as the recurrence relation is common to the assessment of any TC-related risk, such as wind, waves and surges; see for example Vickery and Twisdale (1995), Vickery *et al*. (2000), Willoughby and Rahn (2004) and Powell *et al*. (2005).

In the late 1950s, R.H. Kraft (as referenced by Pfost, 2000, and Kidder *et al*., 2005) used raingauge rainfall depths to estimate the maximum 24-hr rainfall accumulation due to the passage of a TC. According to Kraft, this maximum is 100 inches (254cm) divided by the storm translation speed in knots (1knot = 0.514m/s). Limitations of Kraft's analysis are that it does not provide information on the spatial distribution of rainfall and does not account for TC characteristics such as size and intensity.

Riehl and Malkus (1961), Goodyear (1968) and more recently Simpson and Riehl (1981) have addressed some of these limitations. From the examination of 46 TCs making landfall along the Gulf Coast of the United States, Goodyear (1968) concluded that the 48-hr maximum rainfall depth is about 150mm and occurs 40-80km inland and 40-80km to the right of the storm. Using a similar approach, Riehl and Malkus (1961) and Simpson and Riehl (1981) found that for hurricane-strength cyclones rainfall intensity averages about 33mm/h within 37km from the cyclone center and for larger distances decays almost exponentially. While these studies extend and improve upon Kraft's rule, they too fail to resolve the dependence of rainfall on storm characteristics.

NASA's Tropical Rainfall Measuring Mission (TRMM) (Simpson *et al.*, 1988) produced vast amounts of TC rainfall data, making it possible to conduct more systematic statistical analyses.

Lonfat *et al*. (2004) extracted 2121 tropical cyclone microwave images from the TMI TRMM data set to find how the azimuthally averaged rainfall intensity varies with distance R from the TC center in three storm intensity ranges: tropical storms (TSs) with maximum tangential wind speed V_{max} in the range 18-33m/s; CAT12 cyclones with V_{max} = 34-48m/s and CAT35 cyclones with V_{max} > 49m/s. The study concluded that TC rainfall intensifies with increasing V_{max} and the symmetric component of the rainfall intensity reaches its maximum at a distance from the hurricane center close to the radius of maximum winds R_{max}. For larger distances, rainfall intensity decays approximately as a power law; see their Figure 11. Due mainly to storm translation and vertical wind shear, rainfall intensity lacks circular symmetry and varies also with the azimuth relative to the directions of shear and motion.

Chen *et al*. (2006) used the same TRMM storms to further assess the dependence of rainfall on vertical wind shear S, defined as the difference between the 200 and 850-hPa horizontal wind velocities in the annular region between 200 and 800km from the TC center. The study calculated the average rainfall asymmetry, defined as the ratio of the wavenumber-1 Fourier amplitude to the azimuthal average of the rainfall intensity, for the nine combinations of the 3 intensity categories in Lonfat *et al*. (2004) and three shear magnitude ranges ($S < 5$m/s, $5 \le S \le 7.5$m/s, and $S > 7.5$m/s). Chen *et al*. (2006) found that, in storms in the Northern (Southern) hemisphere with high wind shear ($S > 5$m/s), rainfall intensifies downshear and downshear-left (-right) of the storm.

Parametric rainfall models have also been developed. Using the radial rainfall profiles of Lonfat *et al*. (2004), Tuleya *et al*. (2007) suggested one such model for 24-hr rainfall totals (R-CLIPER) based on climatological and persistence information. The model assumes that storms are symmetric and therefore ignores vertical wind shear and storm motion. Lonfat *et al*. (2007)

built on the R-CLIPER algorithm to construct a parametric rainfall model (PHRaM) that includes shear-related asymmetries according to the results of Chen *et al*. (2006).

Due to data limitations, R-CLIPER and PHRaM use a coarse and incomplete storm parameterization: the effects of storm intensity and vertical wind shear are modeled by interpolating from 3 classes of each variable, the size of the vortex R_{max} is only implicitly taken into account by allowing the location of the maximum rainrate depend on the intensity of the storm according to the results of Lonfat *et al*. (2004), while other factors (e.g. the radial wind velocity profile in the main vortex, the surface roughness, and the storm translation velocity) are ignored. Another limitation is that the Lonfat *et al*. (2004) profiles on which R-CLIPER and PHRaM are based use ensemble averages of storms with significantly different R_{max} values. Since rainfall intensity has a sharp peak near R_{max}, this averaging operation depresses the maximum rainfall estimate. For example, for CAT35 storms Lonfat *et al*. (2004) find maximum rainfall intensities around 12mm/h, which is 2.5-3 times lower than the values most often reported in the literature; see for example Riehl and Malkus (1961), Jiang *et al*. (2006), Trenberth *et al*. (2007) and the rainfall intensities implied by the radar reflectivities in Marks (1985) and Kepert (2006a,b). Finally, the Lonfat *et al*. (2004) profiles are based on TMI rainfall products, which are known to be biased towards low values for high rainfall intensities and towards high values for low rainfall intensities (Viltard *et al.*, 2006).

Here we develop a simple theoretical model of TC rainfall based on the vertical outflow of water vapor from the TC boundary layer (BL). This water vapor flux originates from the low-level convergence of the horizontal flow. The analysis combines a user-specified tangential wind profile at gradient level, an Ekman-type solution for the horizontal and vertical winds inside the boundary layer (BL), and basic thermodynamics. Evaluation of the BL winds is based on Smith's

(1968) axi-symmetric formulation, modified by Langousis *et al*. (2008) to account for storm motion. The resulting models of wind and rainfall are referred to as the modified-Smith (MS) BL model and the modified-Smith-for-rainfall (MSR) model, respectively.

The MSR model produces asymmetric rainfall fields that explicitly depend on: the maximum tangential wind velocity at gradient level V_{max}, the radius of maximum winds R_{max}, Holland's B parameter (Holland, 1980), the surface drag coefficient C_D, the storm translation velocity V_t, the vertical diffusion coefficient of the horizontal momentum K, and the average temperature $\bar{T}$ and saturation ratio $\bar{Q}$ inside the TC boundary layer.

An important departure from previous studies is that we parameterize asymmetries in terms of storm motion not vertical wind shear. The degree to which TC motion and shear contribute to wind, lightning, and rainfall asymmetries has been intensely discussed in the literature; see for example Black *et al*. (2002), Corbosiero and Molinari (2002, 2003), Rogers *et al*. (2003), Lonfat *et al*. (2004) and Chen *et al*. (2006). Separation of the two effects through data analysis is made difficult by the high correlation between the directions and magnitudes of motion and shear in any given geographical region (Corbosiero and Molinari, 2003; Lonfat *et al*., 2004; Chen *et al*., 2006). As a consequence, the calculated rainfall asymmetry is almost the same when storms are aligned in the direction of motion or shear, except for a region-specific rotation; see e.g. Corbosiero and Molinari (2003) and Section 5 below. Another consequence is that, in risk analysis, one may equivalently use shear or motion as conditioning parameter. Since it is easier to include motion than shear when modeling rainfall and the historical records readily provide storm motion information (e.g. Vickery and Twisdale, 1995, and Vickery *et al*., 2000), we have chosen to develop a motion-based rather than shear-based parameterization of rainfall asymmetry.

Section 2 summarizes the boundary layer model developed by Langousis *et al*. (2008) and Section 3 uses the vertical fluxes from that model to estimate surface rainrates in the case of stationary (i.e. symmetric) cyclones. Model predictions are compared to MM5 simulations and R-CLIPER rainrate estimates. The choice of MM5 is based on the fact that this code has been successfully used to simulate a number of TCs, including Hurricanes Bonnie (1998) (Rogers *et al*. 2003, 2007), Floyd (1998) (Tenerelli and Chen, 2001, Rogers *et al*. 2007) and Frances (2004) (Chen *et al*., 2007). Section 4 validates the symmetric MSR predictions using precipitation radar (PR) rainfall products from 38 TRMM frames. The PR rainfall products are less biased than the microwave imager (TMI) data used in previous studies, especially in the core region where rainfall intensities are high (Viltard *et al.*, 2006). Section 5 extends the analysis to translating TCs, which generate asymmetric rainfall fields, assesses the effect of motion on the spatial variation of TC rainfall, and suggests a motion-based parameterization of rainfall asymmetry. Section 6 assesses the sensitivity of the symmetric and asymmetric rainfall components to various TC parameters and Section 7 summarizes the main conclusions.

2. Modified Smith boundary layer model for moving tropical cyclones

A number of studies (Myers and Malkin 1961; Shapiro 1983; Kepert 2001; Langousis *et al*. 2008) have developed theoretical boundary layer (BL) models for moving tropical cyclones. These models derive the radial, tangential and vertical winds inside the boundary layer from an assumed radial profile of the tangential wind velocity under gradient balance, $V_{gr}(R)$, and suitable surface boundary conditions. For example, a widely used gradient wind profile is (Holland, 1980)

$$V_{gr}(R) = V_{max}\sqrt{(R_{max}/R)^{B}\exp[1-(R_{max}/R)^{B}]} \quad (1)$$

where V_{max}, R_{max}, and B are TC-specific parameters. According to equation (1), the tangential velocity V_{gr} increases radially to a maximum V_{max} at $R = R_{max}$ and for $R >> R_{max}$ decays approximately as a power-law of distance with exponent $-B/2$. The shape parameter B varies in the range [1, 2], with typical values around 1.4 (Willoughby and Rahn, 2004). Next we briefly describe the boundary layer model of Langousis *et al*. (2008) and in Sections 3-5 use this model to calculate water vapor fluxes that are responsible for rainfall.

The model of Langousis *et al*. (2008) corrects Smith's (1968) BL formulation for the case of stress surface boundary conditions and accounts for storm motion. Like in Smith (1968), vertical diffusion of the horizontal momentum is parameterized through a vertical diffusion coefficient K. The horizontal momentum equations are written in cylindrical coordinates that move with the storm and solved using the Karman and Pohlhausen momentum integral method. In this method, one specifies vertical profiles for the radial U and tangential V wind velocity components, which satisfy the boundary conditions at the surface (elevation $Z = 0$) and for $Z \to \infty$ tend to the gradient winds, for example the profile in equation (1). The boundary conditions are modeled using a surface stress formulation with drag coefficient C_D.

For U and V, Langousis *et al*. (2008) use functions of the Ekman type with parameters E (amplitude coefficient) and δ (dimensionless BL scale thickness) that vary both radially and azimuthally. The horizontal momentum equations are vertically integrated through the BL to produce a system of two partial differential equations, which are solved numerically to obtain E and δ as functions of radius R and azimuth θ relative to the direction of storm motion. Once the horizontal wind components U and V are obtained, the vertical wind velocity W is calculated using mass conservation, as

$$W(R,\theta,Z) = -\frac{1}{R}\left[\int_0^Z \frac{\partial(RU)}{\partial R}\,dZ + \int_0^Z \frac{\partial V}{\partial \theta}\,dZ\right] \tag{2}$$

For stationary cyclones ($V_t = 0$), there is no azimuthal variation of V and U and equation (2) reduces to

$$W(R,Z) = -\frac{1}{R}\frac{d}{dR}\left(R\int_0^Z U\,dZ\right) \tag{3}$$

$W(R,Z)$ in equation (3) is also the symmetric component of the vertical wind speed for a storm that translates with velocity $V_t \neq 0$.

The above modified Smith (MS) scheme is computationally very efficient and stable over a wide range of parameter values. Model predictions are close to MM5 simulations and to observed wind speeds; see Langousis *et al*. (2008) for details.

3. Estimation of the symmetric component of rainfall

Estimates of rainfall intensity are obtained assuming that, with corrections to be made later, the surface rain rate i is proportional to the water vapor up-flux at a reference height H. Similar approaches have been used in the past to evaluate the rainfall potential of extra-tropical storms (Palmen, 1958), orographic precipitation (Alpert, 1986) and latent heat (Magaki and Barros, 2004), as well as to predict rainfall extremes (Abbs, 1999; Wilson and Toumi, 2005).

To verify how strongly rainfall intensity is related to the vertical velocity $W_H(R,\theta) = W(R,\theta,Z=H)$ from equation (2) at different elevations H, we used MM5 simulations. Figure 1 shows the correlation between the two quantities using 12 frames of Hurricane Frances, simulated at 6 hr intervals for the period Aug. 29-Sep. 01, 2004. The correlation is maximum around 0.85 at an elevation of 2-3km, which can be taken as the reference height H. The inset of

Figure 1 compares the MM5 radial profiles of the simulated rainfall intensity and vertical wind velocity at 3km elevation for the 06:00UTC Aug. 29, 2004 frame. Both profiles are normalized to have unit maximum value. This detailed comparison shows that the correlation coefficient is below 1 due mainly to fluctuations of the rainfall intensity caused by rainbands and other local convective phenomena. If these fluctuations in the MM5 profiles are smoothed out, which is what the present MSR model effectively does, the surface rainfall intensity and vertical wind speed are in even better agreement.

To complete the symmetric rainfall model one needs the proportionality constant between rainfall intensity and vertical wind speed. From simple calculations using a lapse-rate of about 6-7 ^{o}C/km (Rogers and Yau, 1996), one obtains that at elevations in excess of 6-8km the water vapor mixing ratio is close to zero. Consequently, one may accurately assume that the upward water vapor flux from the TC boundary layer equals the downward flux of rainwater. To keep the rainfall model simple, we assume that below the reference height H the temperature T and saturation ratio Q are constant and equal to the depth-averaged values $\bar{T}$ and $\bar{Q}$. For cyclones over tropical and sub-tropical waters, $\bar{T}$ ranges between 20-24^{o}C and $\bar{Q}$ is between 75-85%; see Gray *et al*. (1975), Frank (1977) and Smith (2003). Under these conditions, the symmetric rainfall intensity i_{sym} is given by

$$i_{sym}(R) = \begin{cases} \alpha(\bar{T})\, \bar{Q}\, W_H(R) & , \quad W_H(R) > 0 \\ 0 & , \quad W_H(R) \le 0 \end{cases} \tag{4}$$

where $\alpha(\bar{T})$ is the volume of liquid water per unit volume of saturated air after complete condensation (see below), and $W_H(R) = W(R,Z{=}H)$ is the vertical wind velocity in equation (3) for $Z = H$. The function $\alpha(\bar{T})$ is obtained by combining the ideal gas law with the Clausius-Clapeyron equation. Using a liquid water density ρ_w = 1000kgr/m^3, this gives

$$\alpha(\bar{T}) = \frac{1.324\ 10^{-3}}{\bar{T}+273} \exp\left(\frac{17.67\ \bar{T}}{\bar{T}+243.5}\right) \quad (5)$$

where $\bar{T}$ is in ^{o}C. Notice that in downdraft regions where W_H is negative, equation (4) sets the rainfall intensity to zero. This means that rainfall generation is limited to regions where moist air updrafts. However, due to the slant of the wall updrafts and the cyclonic advection, rainfall may be nonzero also in downdraft regions. This effect is modeled below through a rainfall redistribution scheme.

3.1 Correction for the sloping angle of the wall

Flight observations (e.g. Jorgensen, 1984b; Marks and Houze, 1984) show that the wall updraft of a tropical cyclone slopes outward to altitudes $H_0 \approx$ 5-7km, with an angle ψ_0 from the vertical in the 45^{o}-60^{o} range. The MS model of Langousis *et al.* (2008) assumes fixed vertical profiles of the radial and tangential wind velocities and therefore does not account for such sloping angle. Consequently, equation (4) tends to underpredict the radius of maximum rainfall.

To include radial advection of the rainwater by the wall updraft while avoiding discontinuities in the radial distribution of rainfall, we assume that the angle of the updrafts decreases exponentially with distance R from the storm center, as

$$\psi(R) = \psi_0 \exp\left(-\frac{|R-R_m|}{R_m}\right) \quad (6)$$

where R_m is the location where i_{sym} and W_H in equation (4) are maximum. The outward radial displacement ΔR of the rainwater due to the sloping updrafs is then

$$\Delta R = H_0 \tan\psi \quad (7)$$

Notice that estimating rainfall intensities at distance R from the cyclone center as $i_{sym}(R\text{-}\Delta R)$ is technically incorrect because the model does not satisfy mass conservation. However, we have verified that the error is very small and negligible in practice.

3.2 Comparison with MM5 and R-CLIPER

Figure 2 compares the azimuthally averaged rainfall intensities i_{sym} for Hurricane Frances (2004) estimated by MM5, R-CLIPER (see Introduction), and the present modified-Smith-for-rainfall (MSR) model. The MM5 and MSR curves are the ensemble averages of 12 rainfields simulated at 6 hr intervals during the period Aug. 29-Sep. 01, 2004, using the two models. The MM5 simulations where conducted at 1.67km resolution using the nested grid capability at the University of Miami (Houze *et al*., 2006; 2007), whereas the MSR estimates were obtained as follows:

1) For each frame, the parameters V_{max} and R_{max} in equation (1) were extracted from the azimuthally averaged tangential winds simulated by MM5 at 5km elevation;
2) Holland’s (1980) gradient wind profile with B =1 was used in the model of Langousis *et al*. (2008) to calculate the vertical wind profile $W_H(R)$ at elevation H = 3km;
3) Equations (4) and (5) were used to estimate how the azimuthally averaged rainfall intensity i_{sym} varies with distance R from the TC center;
4) Finally, the results were corrected for sloping-updrafts using equations (6) and (7) and averaged over the 12 frames.

Setting Holland’s B to 1 reproduces well the MM5 rainfall fields, as well as the PR rainfall estimates from TRMM; see Section 4.

The model of Langousis *et al*. (2008) requires also specification of the Coriolis parameter f, the vertical diffusion coefficient K, and the surface drag coefficient C_D. In our simulations we have set f = 4.7 10^{-5} sec^{-1}, which corresponds to latitude 19^o North (the approximate latitude of TC Frances during the period considered), K = $50m^2/s$, and C_D = 0.002. Values of K near $50m^2/s$ are often quoted in the literature (e.g. Smith, 1968; Shapiro, 1983; Kepert, 2001; Kepert 2006b) and are consistent with back-calculations from MM5 simulations (Melicie Desflots, 2007, personal communication). The value 0.002 is representative of drag coefficients extracted from oversea MM5 simulations and to values in the literature for winds in the hurricane range (e.g. Kepert, 2001; Powell *et al*., 2003; Donelan *et al*., 2004). The vertically averaged temperature $\bar{T}$ (over a depth of 3km) and saturation ratio $\bar{Q}$ in equation (4) have been set to 22^oC and 80%, respectively. These values correspond to a depth-averaged mixing ratio of approximately 13gr/kg, which is slightly lower than the ensemble average value of 15gr/Kg extracted from MM5 simulations for Hurricane Frances (Melicie Desflots, 2007, personal communication). For the wall updraft correction in equations (6) and (7), we have assumed an outwards slope of ψ_0 = 50^o from the vertical to an altitude H_0 = 6km.

The solid lines in Figure 2 are the profiles of i_{sym} before the correction for sloping updrafts (thin lines) and after that correction (thick lines). The rainfall estimates from the MSR model are close in shape and magnitude to the MM5 profiles. This is especially true after the correction for out-sloping updrafts. Differences are mostly due to local rainfall intensifications in MM5 caused by rainbands. By contrast, the rain rates of Lonfat *et al*. (2004), which form the basis of the R-CLIPER algorithm, agree with MM5 in the far field but severely underestimate rainfall in the near-core region. As discussed in the Introduction, reasons for the much-reduced rain rate maximum in R-CLIPER are the smoothing effect of ensemble averaging and the bias of the TMI rainfall retrievals used by Lonfat *et al*. (2004).

4. Validation of symmetric MSR predictions

Figure 3 compares PR and MM5 rainfall estimates with rainfall intensities generated by the present MSR model using the procedure described in Section 3. Figure 3.a shows a scatterplot of the ratio between the PR and MSR rainfall estimates as a function of the normalized distance R/R_{max} from the storm center, using a 5km $\times$ 5km grid of spatial locations and the 38 TRMM frames in Table 1 (a total number of 48483 points). The number of points in different ranges of R/R_{max} is shown in Table 2. The MSR estimates where generated using the V_{max}, R_{max} and latitude information in the extended best track record (Demuth *et al*., 2006; M. DeMaria, 2008; personal communication). Figure 3.b shows a similar scatterplot of the ratio between the MM5 and MSR rainfall estimates. In this case the comparison is based on the 12 simulated rainfields of Hurricane Frances, for a total of 43919 points. All MSR simulations were performed using B = 1, K = 50m^2/s and C_D = 0.002. Both Figures 3.a and 3.b show a large dispersion, which reflects the significant small-scale variability of rainfall intensity due to rainbands and local convection. Those fluctuations are not resolved by the MSR model.

Figures 3.c and 3.d show the moving average and standard deviation of the ratios in Figures 3.a and 3.b, using a window of 2000 points. Except for a small region close to the core (R < 1.5R_{max}), the local average in Figure 3.c fluctuates around 1. This means that on average the MSR model generates unbiased rainfall profiles for radial distances up to 15R_{max} from the TC center. For distances R < 1.5 R_{max} the MSR model tends to overpredict the PR rainrates.

As noted above, the large local standard deviations in Figure 3.c reflect the significant small-scale variability of TC rainfall. It is interesting that the standard deviation tends to increase as the distance from the TC center increases. This is in accordance with the findings of other studies

(Jorgensen, 1984a; Powell, 1990, and Molinari *et al*., 1994) that the outer TC environment exhibits more cellular structure and higher small-scale variability relative to the inner region.

Figure 3.d shows that for radial distances up to $8R_{max}$ the MSR model tends to underpredict the MM5 rainfall intensities by about 50%, whereas for larger distances the opposite is true. Since the MSR model displays good skills in reproducing the PR rain rates, it is possible that these differences reflect MM5 biases. This is consistent with what other studies have found when comparing MM5 rainfall estimates to empirical and radar observations; see e.g. Fall *et al.* (2007), Juneng *et al*. (2007), Chen *et al.* (2007) and Rogers *et al*. (2007). The higher standard deviations in Figure 3.d compared to Figure 3.c further suggest that MM5 may enhance local convective activity. One should however caution that these observations are based on just one simulated hurricane and should be validated through a more extensive comparison.

5. Asymmetry of the rainfall field

In the case of a moving TC, equation (4) becomes

$$i(R,\theta) = \begin{cases} \alpha(\bar{T})\ \bar{Q}\ W_H(R,\theta) & , \quad W_H(R,\theta) > 0 \\ 0 & , \quad W_H(R,\theta) \le 0 \end{cases} \tag{8}$$

where the vertical wind speed W_H depends on both R and θ and is given by equation (2) for $Z = H$. In this asymmetric case the rainfall intensities from equation (8) must be corrected both radially using equations (6) and (7) and azimuthally to account for the redistribution of rainwater due to cyclonic circulation; on the latter, see Corbosiero and Molinari (2002), Black *et al*. (2002) and Rogers *et al*. (2003).

To keep the correction simple, we perform the azimuthal redistribution uniformly within an angular interval $[\theta, \theta+\Delta\theta]$ where $\Delta\theta$ is given by

$$\Delta\theta = \frac{V_{gr}(R)}{R}(t_f + t_r) \tag{9}$$

The angle $\Delta\theta$ is in radians (positive clockwise in the Northern hemisphere), V_{gr} is the tangential wind velocity at gradient level (equation (1)), $t_f \approx$ 30min is the time needed for rain generating features like convective cells to develop (Weisman and Klemp, 1986; Rogers and Yau, 1996) and t_r is the time needed for a raindrop at height H to reach the ground. A rough estimate of t_r comes from assuming an average raindrop velocity of 2-3m/s and a boundary layer depth $H \approx$ 2.5-3km. This gives $t_r \approx$ 25min.

Next we use equations (8) and (9) for $t_f + t_r$ = 60min to assess the effect of motion on the spatial variation of TC rainfall and propose a motion-based, rather than shear-based, parameterization of rainfall asymmetry.

5.1. Motion-based versus shear-based parameterization of rainfall asymmetry

MSR is a boundary layer model that generates spatial rainfall without explicitly considering vertical shear S. Rather, rainfall asymmetries are linked to storm motion. Since most of the rainfall originates at low altitudes relative to those that define wind shear, one may expect this to be a suitable approach.

To verify this assertion, Figure 4 compares the shear-aligned rainfall asymmetry from TRMM with the motion-aligned rainfall asymmetry from MSR. In both cases, asymmetry is defined as

$$A(R,\theta) = \frac{i(R,\theta) - i_{sym}(R)}{i_{sym}(R)} \tag{10}$$

where $i(R,\theta)$ is rainfall intensity at (R,θ) and $i_{sym}(R)$ is the azimuthal average. More specifically, Figure 4.a shows the average of the rainfall asymmetries in Figure 7 of Chen *et al*. (2006) over all TC-intensities and shear magnitudes after aligning the shear vector to point North. For shear we have used the distribution in Figure 6 of the same study, whereas for TC intensity we have used the discrete distribution in Table 1 of Lonfat *et al*. (2004).

Similarly, Figure 4.b was generated by averaging rainfall asymmetries from the MSR model over a range of TC intensities and translation velocities. Storms are assumed to move in the Northern hemisphere at an angle of 75^o west of the shear-direction in Figure 4.a. This is the average angle between shear and motion from Figures 3 and 12 of Chen *et al*. (2006) and is in the range reported by Corbosiero and Molinari (2003). For storm intensity we have used the same discrete distribution as in Figure 4.a, setting V_{max} = 30m/s for tropical storms, V_{max} = 42m/s for CAT12 and V_{max} = 60m/s for CAT35 systems. The distribution of the translation velocity was taken from Figure 11 of Chen *et al*. (2006). All other storm parameters have been kept constant, with values $f = 4.7\ 10^{-5}$ sec^{-1}, R_{max} = 40km, $B = 1$, $\bar{T} = 22^o$C, $\bar{Q} = 0.8$, $K = 50$m^2/s, and C_D =0.002.

One sees that the two asymmetries are very similar in both pattern and magnitude, validating the contention that for rainfall risk one can use the MSR model with motion as the driver of asymmetry. Differences between Figures 4.a and 4.b occur mainly far away from the core (R > 250km), but these differences are statistically not significant and inconsequential for risk analysis.

6. Sensitivity analysis

Figures 5 and 6 show the sensitivity of the MSR model results to various tropical cyclone characteristics: the tangential wind speed under gradient balance (parameterized by V_{max}, R_{max} and B; see equation (1)), the vertical diffusion coefficient K, the surface drag coefficient C_D, the depth-averaged temperature $\bar{T}$ inside the BL and the translation velocity V_t of the storm. Since rainfall intensity is proportional to the depth-averaged saturation ratio $\bar{Q}$ (see equations (4) and (8)), dependence on $\bar{Q}$ is not illustrated.

Figure 5 shows the sensitivity of the azimuthally averaged rainfall intensity i_{sym} to V_{max}, R_{max}, B, K, C_D and $\bar{T}$. Parameters are varied one at a time around the base-case values V_{max} = 50m/s, R_{max} = 40km, B = 1, K = 50m^2/s, C_D = 0.002, $\bar{T}$ = 22^{o}C and $\bar{Q}$ = 0.8 (solid lines). The figure shows that the maximum tangential velocity V_{max} and the roughness of the surface boundary (expressed through C_D) have significant effects on rainfall intensity and that lower values of R_{max} produce rain rates that are more peaked and more concentrated near the TC center.

Dependence of the azimuthally averaged rainrate i_{sym} on V_{max} of the type produced by the model has been observed in TC rainfall data (Lonfat *et al.*, 2004, Tuleya *et al.*, 2007; see Introduction). For example, the expressions used by the R-CLIPER parameterization (Tuleya *et al.*, 2007) indicate that when V_{max} increases from 50 to 70m/s, the maximum rainrate increases by a factor of about 1.5. This is also what the MSR model predicts. However, to our knowledge the effect of C_D and R_{max} on i_{sym} have not been isolated from data. The effect of surface roughness can be qualitatively assessed using the finding in Trenberth *et al.* (2007) that low-level horizontal wind convergence is by far the dominant factor for TC rainfall. Hence, if one considers that low-level convergence increases with increasing surface drag (Shapiro, 1983; Kepert, 2001; Langousis *et al.*, 2008), one concludes that higher surface drag coefficients should cause TC rainfall to intensify.

The B parameter has a small effect on the peak rainfall intensity, but influences significantly the rate at which rainfall decays with radial distance (higher values of B resulting in faster decay). The azimuthally averaged rainfall intensity i_{sym} has small sensitivity to temperature $\bar{T}$ and the vertical diffusion coefficient K. Consequently, setting those parameters to constant values (e.g. to $\bar{T}$ = 22^{o}C and K = 50m^2/s, as was done in Sections 3-5) does not induce large errors.

Figure 6 shows the effect of the drag coefficient C_D and translation velocity V_t on rainfall asymmetry for a TC that translates northward in the Northern hemisphere. All other parameters are the same as for the base case in Figure 5. As expected and in accordance with findings in Lonfat *et al*. (2004), the asymmetry increases as V_t increases. The effect of C_D is more complex: at the front of the storm, rainfall asymmetry is insensitive to C_D, whereas at the rear-right the rainfall asymmetry increases with decreasing C_D.

7. Conclusions

We have developed a simple theoretical model for the large-scale rainfall intensity field generated by translating tropical cyclones (TCs). The model assumes that, with corrections for sloping updrafts and azimuthal redistribution, the upward water vapor flux originated from the boundary layer is a good predictor of rainfall intensity. Vertical moisture fluxes are calculated using elementary thermodynamic principles in combination with a boundary layer model that extends Smith's (1968) analysis to moving storms.

The proposed modified-Smith-for-rainfall (MSR) model estimates the rainfall field from a given radial profile of the tangential wind speed at gradient level, the translation velocity V_t of the storm, the surface drag coefficient C_D, and the average temperature $\bar{T}$ and saturation ratio $\bar{Q}$ inside the TC boundary layer. Model predictions are compared to MM5 simulations and R-CLIPER estimates and validated through precipitation radar (PR) rainfall products from TRMM. The MSR model displays good skills in reproducing the shape and magnitude of PR rainfall fields. We have also verified that the asymmetries produced by storm motion are close to those observed and often parameterized in terms of vertical wind shear. In a parametric analysis, we have studied how the model predictions depend on various storm characteristics.

The combination of a rich parameterization and computational efficiency makes the present model an attractive instrument for risk applications, where one must assess tropical cyclone rainfall under many storm and environmental scenarios. For the latter purpose one needs tools with computational times on the order of minutes. This constraint effectively rules out the use of full-physics high-resolution numerical weather prediction models. An important limitation of the MSR model relative to high-resolution schemes is that it does not account for local rainfall intensifications due to rainbands and local convection. As was explained in the Introduction, these phenomena contribute to the "residuals" of the present model, which for risk analysis must be modeled statistically. This is the focus of an upcoming manuscript. Another limitation of the MSR model is that it does not account for after-landfall conditions and therefore is applicable only to open-water or near-water sites. Extension of the model to inland conditions should be pursued in the future.

Acknowledgments

This work was supported by the Alexander S. Onassis Public Benefit Foundation under Scholarship No. F-ZA 054/2005-2006. The authors are grateful to Melicie Desflots for the MM5 simulations, Shuyi Chen for the PR-TRMM rainfall products, Robert Rogers for providing parametric expressions for the shear-induced rainfall asymmetries, and Mark DeMaria for access to the extended best track record. We further thank Jim Hansen for useful discussions and two anonymous reviewers for their constructive comments.

References

Abbs, D.J. (1999) A numerical modelling study to investigate the assumptions used in the calculation of probable maximum precipitation, *Water Resour. Res.*, **35**, 785–796.

Alpert, P. (1986) Mesoscale indexing of the distribution of orographic precipitation over high mountains, *J. Clim. Appl. Meteor.*, **25**, 532-545.

Black, M.L., J.F. Gamache, F.D. Marks Jr., C.E. Samsury, and H.E. Willoughby (2002) Eastern Pacific Hurricanes Jimena of 1991 and Olivia of 1994: The effect of vertical shear on structure and intensity, *Mon. Wea. Rev.*, **130**(9): 2291-2312.

Chen, S.S., J.F. Price, W. Zhao, M.A. Donelan, and E.J. Walsh (2007) The CBLAST-hurricane program and the next-generation fully coupled atmosphere-wave-ocean models for hurricane research and prediction, *Bull. Amer. Meteor. Soc.*, **88**: 311-317.

Chen, S.S., M. Lonfat, J.A. Knaff, and F.D. Marks, Jr. (2006) Effects of vertical wind shear and storm motion on tropical cyclone rainfall asymmetries deduced from TRMM, *Mon. Wea. Rev*., **134**: 3190-3208.

Corbosiero, K.L., and J. Molinari (2002) The effects of vertical wind shear on the distribution of convection in tropical cyclones, *Mon. Wea. Rev.,* **130**: 2110–2123.

Corbosiero, K.L., and J. Molinari (2003) The relationship between storm motion, vertical wind shear, and convective asymmetries in tropical cyclones, *J. Atmos. Sci.*, **60**: 366–376.

Demuth, J., M. DeMaria, and J.A. Knaff (2006) Improvement of advanced microwave sounder unit tropical cyclone intensity and size estimation algorithms, *J. Appl. Meteor.*, **45**, 1573-1581.

Donelan, M.A., B.K. Haus, N. Reul, W.J. Plant, M. Stiassnie, H.C. Graber, O.B. Brown, and E.S. Saltzman (2004) On the limiting aerodynamic roughness of the ocean in very strong winds, *Geophys. Res. Lett.,* **31***,* L18306, doi:10.1029/2004GL019460.

Fall, S., D. Niyogi, U.C. Mohanty, and A. Kumar (2007) Application of weather prediction models for hazard mitigation planning: a case study of heavy off-season rains in Senegal, *Nat. Hazards*, **41**, 227–243, doi:10.1007/s11069-006-9033-x

Frank, W.M. (1977) The structure and energetics of the tropical cyclone: I. Storm structure, *Mon. Wea. Rev.*, **105**: 1119-1135.

Goodyear, H.V. (1968) Frequency and areal distributions of tropical storm rainfall in the United States coastal region on the Gulf of Mexico, ESSA Tech. Rep. WB-7, Washington, DC, 48 pp. [Available from NOAA Miami Regional Library, Atlantic Oceanographic and Meteorological Laboratory (AOML), 4301 Rickenbacker Causeway Miami, FL 33149.]

Gray, W.M., E. Ruprecht, and R. Phelps (1975) Relative humidity in tropical weather systems. *Mon. Wea. Rev.*, **103**:685-690.

Holland, G.J. (1980) An analytic model of the wind and pressure profiles in hurricanes, *Mon. Wea. Rev.*, **108**: 1212-1218.

Houze, R.A., S.S. Chen, and co-authors (2006) The hurricane rainband and intensity change experiment (RAINEX): Observations and modeling of Hurricanes Katrina, Ophelia, and Rita (2005), *Bull. Amer. Meteor. Soc*, **87**: 1503-1521.

Houze, R.A., S.S. Chen, B. Smull, W.-C. Lee, and M. Bell (2007) Hurricane intensity and eyewall replacement, *Science*, **315**: 1235-1239.

Jiang, H., P.G. Black, E.J. Zipser, F.D. Marks Jr., and E.W. Uhlhorn (2006) Validation of rain rate estimation in hurricanes from the stepped frequency microwave radiometer: Algorithm correction and error analysis, *J. Atmo. Sci.*, **63**(1): 252-267.

Jorgensen, D.P. (1984a) Mesoscale and convective-scale characterisitcs of mature hurricanes. Part I: General observations by research aircraft, *J. Atmo. Sci.*, **41**(8), 1268-1286.

Jorgensen, D.P. (1984b) Mesoscale and convective-scale characterisitcs of mature hurricanes. Part II: Inner core structure of Hurricane Allen (1980), *J. Atmo. Sci.*, **41**(8): 1287-1311.

Juneng, L., F.T. Tangang, C.J.C. Reason, S. Moten, and W.A.W. Hassan (2007) Simulation of tropical cyclone Vamei (2001) using the PSU/NCAR MM5 model, *Meteorol. Atmos. Phys.*, **97**, 273–290, doi: 10.1007/s00703-007-0259-2

Kepert, J. (2001) The dynamics of boundary layer jets within the tropical cyclone core. Part I: Linear theory, *J. Atmo. Sci*, **58**: 2469-2484.

Kepert, J. (2006a) Observed boundary layer wind structure and balance in the hurricane core. Part I: Hurricane Georges, *J. Atmo. Sci*, **63**: 2169-2193.

Kepert, J. (2006b) Observed boundary layer wind structure and balance in the hurricane core. Part II: Hurricane Mitch, *J. Atmo. Sci*, **63**:2194-2211.

Kidder, S.Q., S.J. Kusselson, J.A. Knaff, R.R. Ferraro, R.J. Kuligowski, and M. Turk (2005) The tropical rainfall potential (TRaP) technique. Part I, *Wea. Forecasting*, **20**: 456–464.

Landsea, C.W. (2000) Climate variability of tropical cyclones, In: *Storms*, Vol.1, Edited by: R. Pielke, Jr. and R. Pielke, Sr., Routledge, NY.

Langousis, A., D. Veneziano, and S. Chen (2008) Boundary layer model for moving tropical cyclones, In: *Hurricanes and Climate Change*, Edited by: J. Elsner and T.H. Jagger, Springer (in press).

Lonfat, M., F.D. Marks, Jr. and S.S. Chen (2004) Precipitation distribution in tropical cyclones using the tropical rainfall measuring mission (TRMM) microwave imager: A global perspective, *Mon. Wea. Rev.*, **132**: 1645-1660.

Lonfat, M., R. Rogers, T. Marchok, and F.D. Marks Jr. (2007) A parametric model for predicting hurricane rainfall, *Mon. Wea. Rev.*, **135**: 3086-3097.

Magagi, R., and A.P Barros (2004) Estimation of latent heating of rainfall during the onset of the Indian monsoon using TRMM PR and radiosonde data, *J. Appl. Meteor.*, **43**, 328-349.

Marks, F. D. Jr., L.K. Shay, and PDT-5 (1998) Landfalling tropical cyclones: Forecast problems and associated research opportunities, *Bull. Amer. Meteor. Soc.*, **79**: 305-323.

Marks, F.D. Jr. (1985) Evolution of the structure of precipitation in Hurricane Allen (1980), *Mon. Wea. Rev.*, **113**: 909-930.

Marks, F.D. Jr., and R.A. Houze Jr. (1984) Airborne Doppler radar observations in Hurricane Debby, *Bull. Amer. Meteor. Soc.*, **65**: 569-582.

Marks, F.D. Jr., and R.A. Houze Jr. (1984a) Airborne Doppler radar observations in Hurricane Alicia. Preprints, 22nd Conference on Radar Meteorology, Zurich, Switzerland, American Meteorological Society, Boston, 578-583.

Molinari, J., P.K. Moore, V.P. Idone, R.W. Henderson and A.B. Saljoughy (1994) Cloud-to-ground lightning in hurricane Andrew, *J. Geophys. Res.*, **99**, 16 665-16 676.

Myers, V.A., and W. Malkin (1961) Some properties of hurricane wind fields as deducted from trajectories. NHRP Rep. 49, 45pp. [NOAA/NHRL Library, 1320 South Dixie Highway, Coral Gables, FL 33146].

Palmen, E. (1958) Vertical circulation and release of kinetic energy during the development of hurricane Hazel into an extratropical storm, *Tellus*, **10**(1), 1-23.

Pfost, R.L. (2000) Operational tropical cyclone quantitative precipitation forecasting, *Natl. Wea. Dig.*, **24**: 61–66.

Powell, M.D. (1990) Boundary layer structure and dynamics in outer hurricane rainbands. Part I: mesoscale rainfall and kinematic structure, *Mon. Wea. Rev.*, **118**, 891-917.

Powell, M., G. Soukup, S. Cocke, S. Gulati, N. Morisseau-Leroy, S. Hamid, N. Dorst and L. Axe, (2005) State of Florida Hurricane Loss Projection Model: Atmospheric Science Component, *J. Wind Engineering and Industrial Aerodynamics,* **93**: 651-674.

Powell, M.D., P.J. Vickery, and T.A. Reinhold (2003) Reduced drag coefficient for high wind speeds in tropical cyclones, *Nature*, **422**, 279–283.

Rappaport, E.N. (2000) Loss of life in the United States associated with recent Atlantic tropical cyclones, *Bull. Amer. Meteor. Soc.,* **81**: 2065-2074.

Riehl, H., and J. Malkus (1961) Some aspects of Hurricane Daisy (1958), *Tellus*, **13**: 181–213.

Rogers, R., S. Chen, J. Tenerelli, H. Willoughby (2003) A numerical study of the impact of vertical wind shear on the distribution of rainfall in Hurricane Bonnie, *Mon. Wea. Rev.*, **131**: 1577-1599.

Rogers, R.F., M.L. Black, S.S. Chen, and R.A. Black (2007) An Evaluation of Microphysics Fields from Mesoscale Model Simulations of Tropical Cyclones. Part I: Comparisons with Observations, *J. Atmos. Sci.*, **64**: 1811–1834.

Rogers, R.R., and M.K. Yau (1996) *A Short Course in Cloud Physics*, Third Edition, Butterwirth Heinemann, U.S.A.

Shapiro, L.J. (1983) The asymmetric boundary layer flow under a translating hurricane. *J. Atmos. Sci.*, **40**: 1984-1998.

Simpson, J., R.F. Adler, and G.R. North (1988) Proposed tropical rainfall measuring mission (TRMM) satellite, *Bull. Amer. Meteor. Soc.*, **69**: 278-295.

Simpson, R.H., and H. Riehl (1981) *The Hurricane and Its Impact*, Louisiana State University Press, 398 pp.

Smith, R.K. (1968) The surface boundary layer of a hurricane, *Tellus*, **20**: 473-484.

Smith, R.K. (2003) A simple model of the hurricane boundary layer, *Quart. J. Roy. Met. Soc.*, **129**: 1007-1027.

Tenerelli, J.E., and S.S. Chen (2001), High-resolution simulation of Hurricane Floyd (1999) using MM5 with a vortex-following mesh refinement. *Preprints, 18th Conference on Weather Analysis and Forecasting/14th Conference on Numerical Weather Prediction,* 30 July-2 August 2001, Ft. Lauderdale, Florida, AMS, J54-J56.

Trenberth, K.E., C.A. Davis, and J. Fasullo (2007) The water and energy budgets of hurricanes: Case studies of Ivan and Katrina, *J. Geophys. Res.*, doi:10.1029/2006JD008303.

Tuleya, R.E., M. DeMaria, and J.R. Kuligowski (2007) Evaluation of GFDL and simple statistical model rainfall forecasts for U.S. landfalling tropical storms, *Wea. Forecasting*, **22**: 56–70.

Vickery, P.J. and L.A. Twisdale (1995), Prediction of hurricane wind speeds in the United States, *J. of Structural Engineering*, **121**(11): 1691-1699.

Vickery, P.J., P.F. Skerlj, and L.A. Twisdale (2000) Simulation of hurricane risk in the U.S. using empirical track model, *J. of Structural Engineering*, **126**(10): 1222-1237.

Viltard, N., C. Burlaud, and C. Kummerow (2006) Rain retrieval form TMI brightness temperature measurements using a TRMM PR – based data base, *J. Applied Meteor. and Climat.*, **45**: 455-466.

Weisman, M.L., and J.B. Klemp (1986) Characteristics of isolated convective storms, In: *Mesoscale Meteorology and Forecasting*, Edited by: Ray P.S., *Amer. Meteor. Soc.*, Boston, U.S.A.

Willoughby, H.E., and M.E. Rahn (2004) Parametric representation of the primary hurricane vortex. Part I: Observations and evaluation of the Holland (1980) model, *Mon. Wea. Rev.*, **132**: 3033-3048.

Wilson, P.S., and R. Toumi (2005) A fundamental probability distribution for heavy rainfall, *Geophys. Res. Lett.*, **32**, L14812, doi:10.1029/2005GL022465.

Table 1: Storm characteristics for the PR-TRMM rainfields used in Figure 3. The estimates of V_{max} and R_{max} are obtained from the extended best track record (M. DeMaria, 2008; personal communication).

	Storm center		V_{max} (m/s)	R_{max} (km)	Intensity category
	Lat. (deg)	Lon. (deg)			
Floyd '99	21.7	-61.6	48.8	41	CAT2
	23.5	-68.7	64.0	37	CAT4
	23.7	-70.6	69.3	37	CAT4
Frances '04	12.6	-43.7	23.1	37	TS
	15.7	-49.8	51.4	19	CAT3
	17	-51.3	54.0	28	CAT3
	17.9	-52.6	59.1	28	CAT4
	19	-57.3	51.4	28	CAT3
	21.2	-68.5	61.7	28	CAT4
Ivan '04	8.9	-38.9	25.7	37	TS
	10.7	-50.6	57.5	28	CAT4
	11.2	-53.4	51.4	28	CAT3
	12.3	-64.1	61.7	19	CAT4
	12.7	-66.2	61.7	20	CAT4
	17.4	-77.3	66.8	28	CAT4
	17.7	-78.4	64.3	28	CAT4
	25.6	-87.4	61.7	46	CAT4
Jeanne '04	27.4	-70.6	38.6	42	CAT1
	25.5	-69.5	41.1	37	CAT2
	26.5	-74.3	43.7	60	CAT2
	26.5	-75.6	46.3	46	CAT2
Karl '04	11.5	-35.3	26.7	37	TS
	17.3	-45.5	57.8	32	CAT3
	19.1	-47.4	64.0	32	CAT4
	22.9	-48.6	54.0	28	CAT3
	25.7	-49.5	48.8	28	CAT3
Katrina '05	24.6	-85.6	51.5	56	CAT3
	25	-86.2	56.5	50	CAT3
	26.9	-89	75.0	38	CAT5
Lilli '02	23.6	-87.2	51.5	20	CAT2
	24.4	-88.4	56.5	20	CAT2
	28.4	-91.4	54.0	20	CAT4
	29	-91.9	41.1	20	CAT2
Rita '05	24.3	-85.9	61.7	28	CAT4
	24.9	-88	77.1	19	CAT5
	25.4	-88.7	72.0	19	CAT5
	26.8	-91	59.1	37	CAT4
	27.4	-91.9	59.1	37	CAT4

Table 2: Number of data shown in Figure 3.a that fall into different ranges of R/R_{max}.

***R*/*R*$_{max}$ range**	***No. of data points***
0-1.5	3586
1.5-3	8772
3-4.5	11025
4.5-6	9250
6-7.5	6626
7.5-9	4027
9-10.5	2272
10.5-12	1273
12-19	1652

Figure captions

Figure 1: (a) Ensemble correlation function of the vertical wind velocity at different elevations and the surface rainfall intensity from MM5 simulations of Hurricane Frances. Ensemble averaging is over 12 frames (at 6 hr intervals) during the period Aug. 29-Sep. 01, 2004. (b) Normalized radial profiles of surface rainfall intensity and vertical wind velocity on Aug. 29, 2004 at 06:00UTC at 3km elevation.

Figure 2: Comparison of the ensemble average rainrates for Hurricane Frances 2004 during the period Aug. 29-Sep. 01, produced by the MSR, MM5 and R-CLIPER rainfall models.

Figure 3: Comparison of PR, MM5 and MSR point rainfall intensity estimates. (a) Scatterplot of the ratio between PR and MSR rainfall estimates as a function of the normalized distance R/R_{max} from the storm center, for 38 TRMM frames; see Table 1. The number of data points in different ranges of R/R_{max} is shown in Table 2. (b) Scatterplot of the ratio between MM5 and MSR rainfall estimates as a function of R/R_{max}, for hurricane Frances 2004 during the period Aug. 29-Sep. 01. (c) Local averages and standard deviation of the ratios in (a) using a moving window of 2000 points. (d) Same as (c) but for the ratios in (b).

Figure 4: Comparison of rainfall asymmetry from TRMM and the MSR model. (a) Ensemble average of rainfall asymmetries in Figure 7 of Chen *et al*. (2006) over all TC intensities and shear magnitudes. (b) Ensemble average of rainfall asymmetries from MSR over all TC intensities and translation velocities. In (b), the TC moves in the Northern hemisphere at an angle 75^o to the west of the shear vector in (a).

Figure 5: Sensitivity of the azimuthally averaged MSR rainfall profiles. Solid lines correspond to V_{max} = 50m/s, R_{max} = 40km, B = 1, C_D = 0.002, K = 50m^2/s, $\bar{T}$= 22^{o}C and $\bar{Q}$= 0.8. Each panel shows results under perturbation of one parameter.

Figure 6: Sensitivity of MSR rainfall asymmetry to the drag coefficient C_D and the storm translation velocity V_t for a tropical cyclone that moves northward. All other parameters are the same as for the base case in Figure 5.

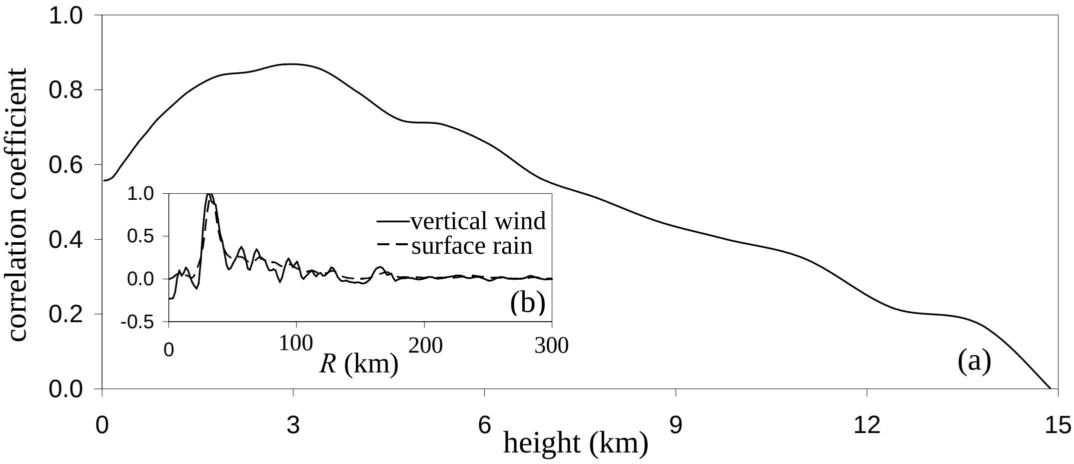

Figure 1: (a) Ensemble correlation function of the vertical wind velocity at different elevations and the surface rainfall intensity from MM5 simulations of Hurricane Frances. Ensemble averaging is over 12 frames (at 6 hr intervals) during the period Aug. 29-Sep. 01, 2004. (b) Normalized radial profiles of surface rainfall intensity and vertical wind velocity on Aug. 29, 2004 at 06:00UTC at 3km elevation.

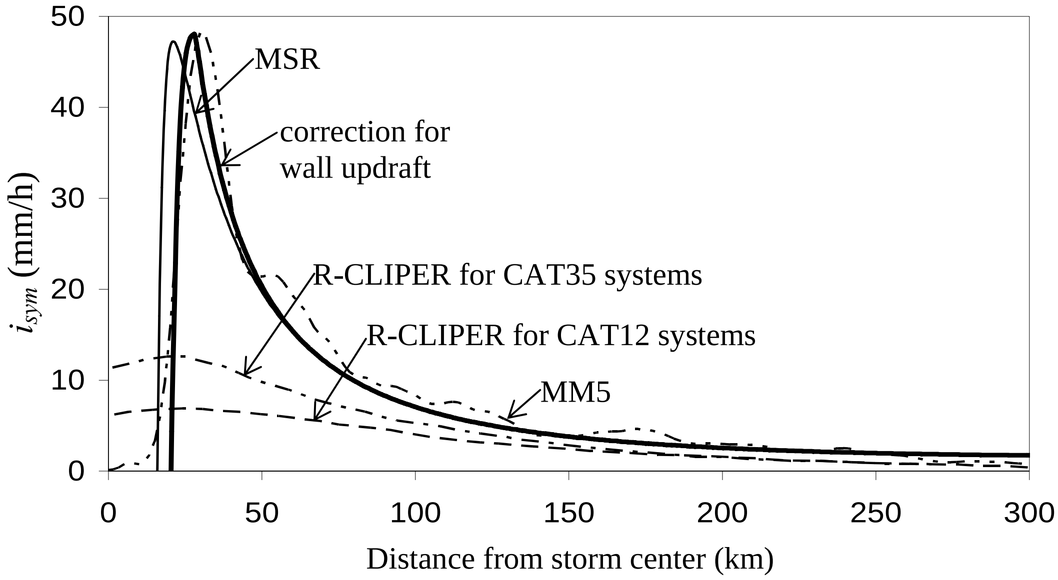

Figure 2: Comparison of the ensemble average rainrates for Hurricane Frances 2004 during the period Aug. 29-Sep. 01, produced by the MSR, MM5 and R-CLIPER rainfall models.

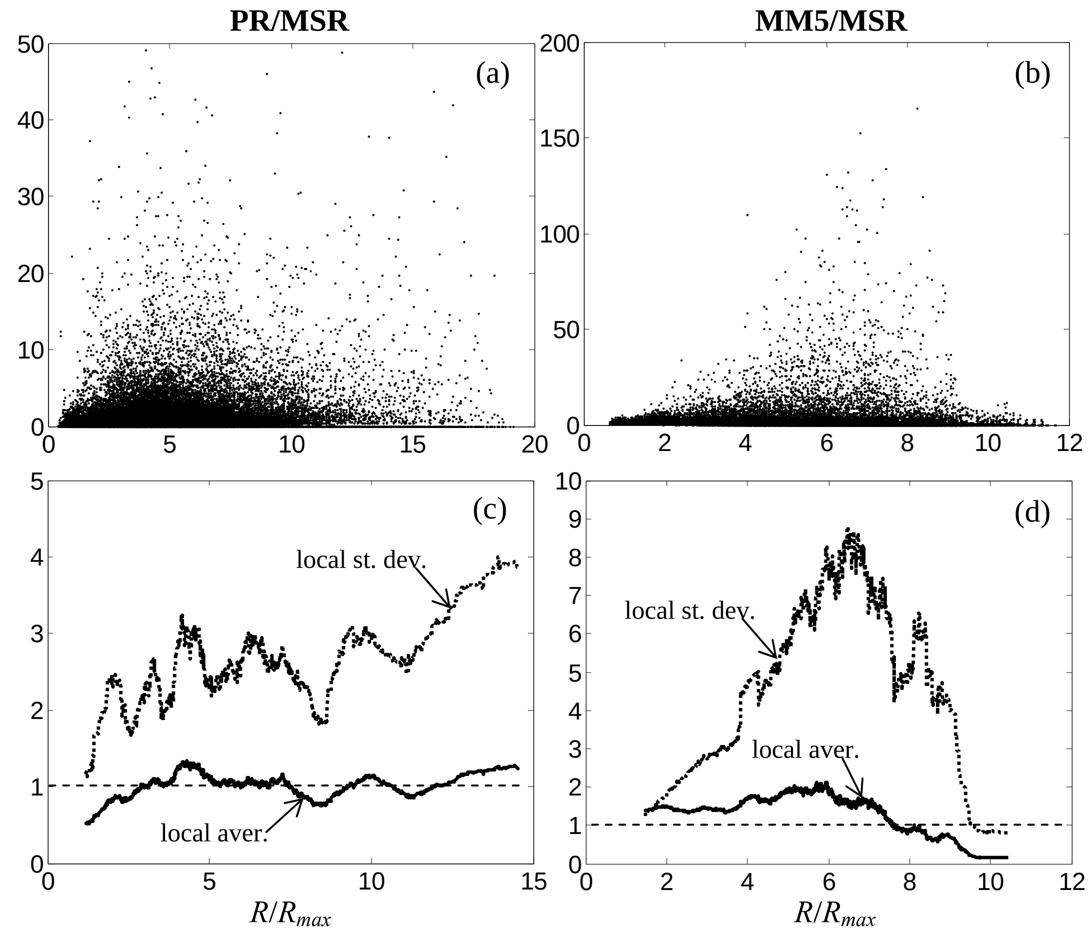

Figure 3: Comparison of PR, MM5 and MSR point rainfall intensity estimates. (a) Scatterplot of the ratio between PR and MSR rainfall estimates as a function of the normalized distance R/R_{max} from the storm center, for 38 TRMM frames; see Table 1. The number of data points in different ranges of R/R_{max} is shown in Table 2. (b) Scatterplot of the ratio between MM5 and MSR rainfall estimates as a function of R/R_{max}, for hurricane Frances 2004 during the period Aug. 29-Sep. 01. (c) Local averages and standard deviation of the ratios in (a) using a moving window of 2000 points. (d) Same as (c) but for the ratios in (b).

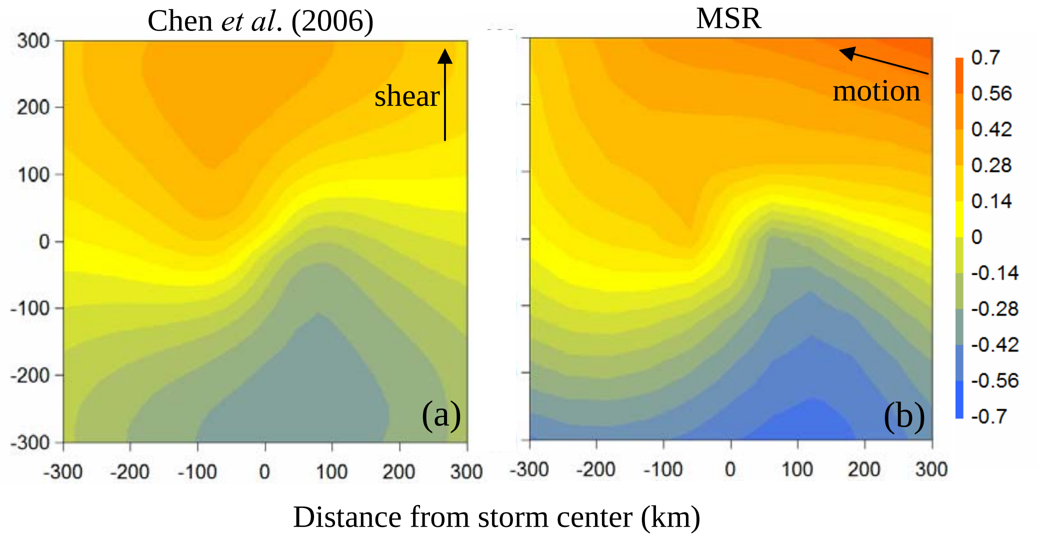

Figure 4: Comparison of rainfall asymmetry from TRMM and the MSR model. (a) Ensemble average of rainfall asymmetries in Figure 7 of Chen *et al*. (2006) over all TC intensities and shear magnitudes. (b) Ensemble average of rainfall asymmetries from MSR over all TC intensities and translation velocities. In (b), the TC moves in the Northern hemisphere at an angle 75^{o} to the west of the shear vector in (a).

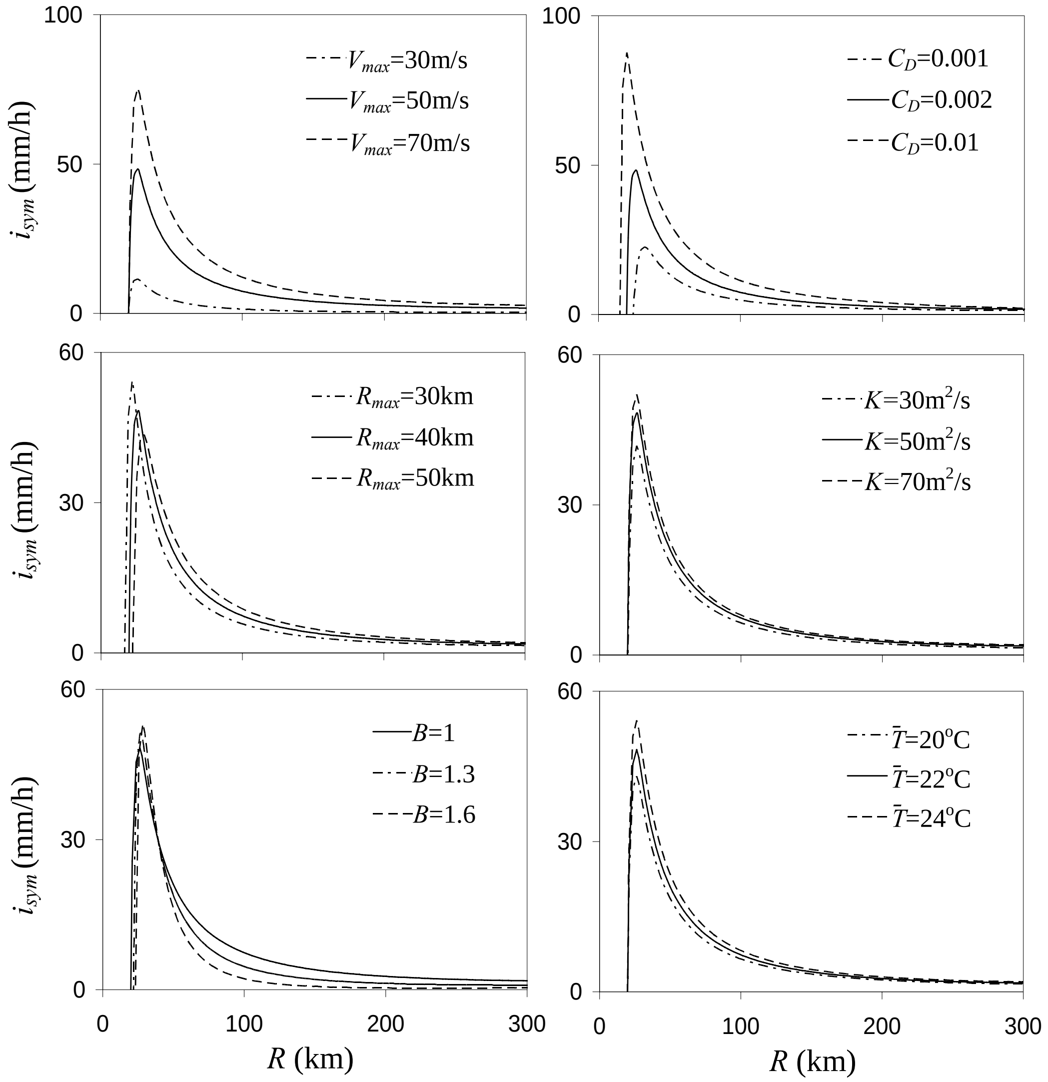

Figure 5: Sensitivity of the azimuthally averaged MSR rainfall profiles. Solid lines correspond to V_{max} = 50m/s, R_{max} = 40km, B = 1, C_D = 0.002, K = 50m^2/s, T = 22^{o}C and Q = 0.8. Each panel shows results under perturbation of one parameter.

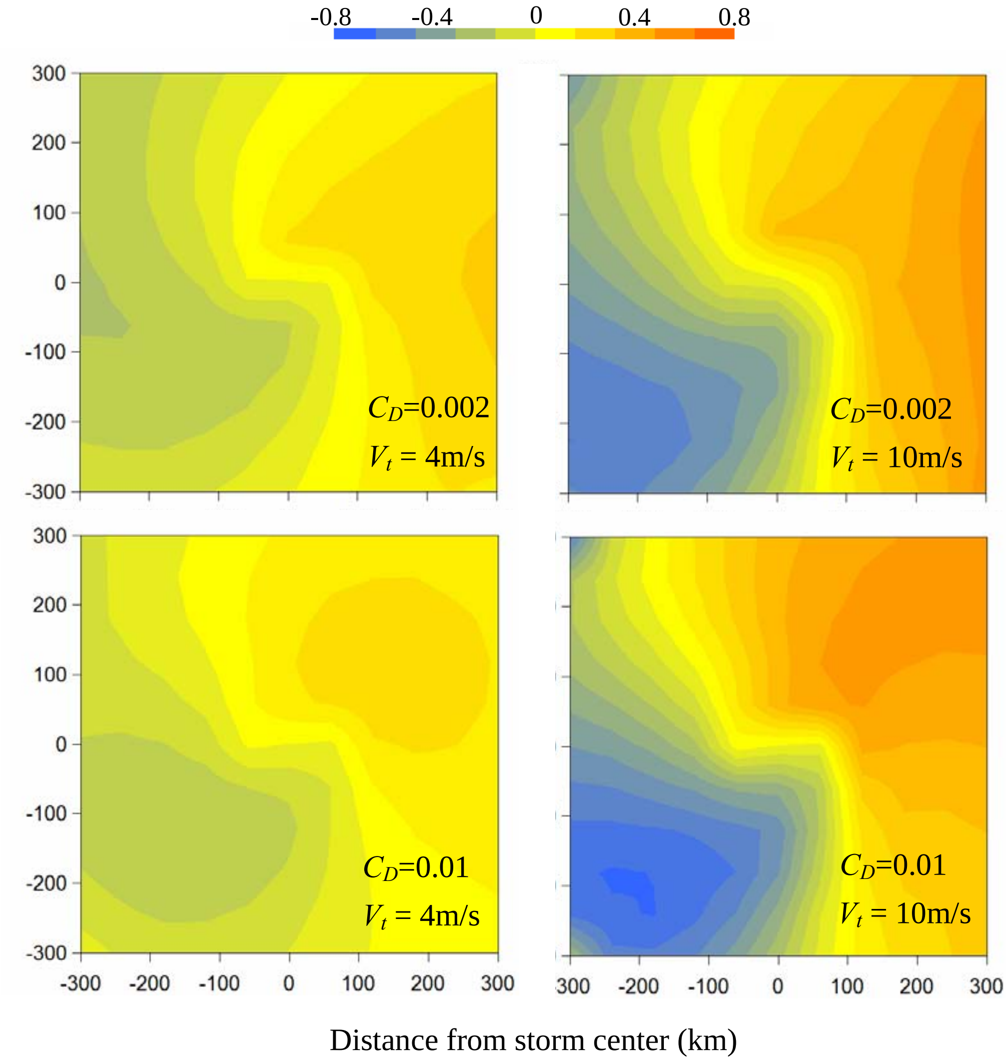

Figure 6: Sensitivity of MSR rainfall asymmetry to the drag coefficient C_D and the storm translation velocity V_t for a tropical cyclone that moves northward. All other parameters are the same as for the base case in Figure 5.